Doping and its efficiency in a-SiO_x:H

Andreas Janotta,* Rainer Janssen, Matthias Schmidt, Tobias Graf, and Martin Stutzmann
Walter Schottky Institut, Technische Universität München, Am Coulombwall, 85748 Garching, Germany

Lutz Görgens, Andreas Bergmaier, and Günther Dollinger
Physik Department E 12, Technische Universität München, James-Franck-Strasse, 85748 Garching, Germany

Claus Hammerl, Sascha Schreiber, and Bernd Stritzker
Institut für Physik, Universität Augsburg, 86135 Augsburg, Germany

(Received 29 July 2003; revised manuscript received 4 November 2003; published 15 March 2004)

Amorphous hydrogenated silicon suboxides (a-SiO_x:H) deposited by plasma enhanced chemical vapor deposition have a band gap which can be tuned from 1.9 to 3.0 eV by varying the oxygen content [O] from 0 to 50 at. %. n- and p-type doping is realized by adding PH_3 and B_2H_6, respectively, to the source gases SiH_4, H_2, and CO_2. Alloying with increasing amounts of oxygen reduces the average coordination number $\langle r\rangle$ from a value close to 4 (a-Si:H) to ≈ 2.7, which gradually approaches the ideal value of $\langle r\rangle = 2.4$ for network glasses. This goes along with a softening of the amorphous SiO_x network, i.e., a reduction of the mechanical hardness of the material, which is also predicted by rigidity percolation theory. Also the incorporation of dopant atoms into electrically active, fourfold coordinated sites becomes more unlikely with increasing [O]. As a consequence, n- and p-type doped SiO_x shows increasingly intrinsic character for higher oxygen concentrations. Doping fails for values of $\langle r\rangle < 3$ and the doping efficiency tends towards zero. Thus, an overall fourfold coordination was found to be a crucial requirement for efficient doping in amorphous semiconductors.

DOI: 10.1103/PhysRevB.69.115206 PACS number(s): 61.43.Dq, 68.55.Ln, 68.55.Nq, 71.55.Jv

I. INTRODUCTION

For a long time in the history of amorphous silicon (a-Si), substitutional doping was believed to be impossible due to the flexibility of the disordered network. The 8-N rule proposed by Mott[1,2] conjectured that every atom in an amorphous solid should be incorporated with its preferred chemical valency. This rule implies the complete absence of topological constraints in a random covalent network. However, Phillips[3–5] argued that the average coordination of an ideal glass is $\langle r\rangle = 2.4$. Thus, four-valent silicon must inevitably be topologically constrained due to its higher coordination. These constraints in a-Si readily account for the existence of threefold coordinated silicon dangling bonds[6] which otherwise would contradict the 8-N rule.

Accordingly, the 8-N rule suggests that group III (B) and V (P or As) dopants are threefold coordinated, as shown exemplarily in Fig. 1(b) for phosphorus. This configuration leads to additional occupied states in the valence band and is electronically inactive. Active donor and acceptor levels, instead, would require a fourfold, substitutional coordination, as shown in Fig. 1(a) for phosphorus. In contrast to these predictions, substitutional n- and p-type doping of hydrogenated amorphous silicon (a-Si:H) was observed experimentally,[7–9] constituting further exceptions from the 8-N rule. However, for a significant shift of the Fermi level towards the band edges, dopant concentrations up to ≈ 1 at. % are necessary and the doping efficiency decreases strongly to a few percent with increasing dopant concentration.[10,11] Additionally, large numbers of charged defects are created. These facts can be understood phenomenologically by a modification of the 8-N rule to include charged atoms and based on thermal equilibration processes between certain structural configurations:[10]

$$\mathrm{Si}_4^0 + \mathrm{P}_3^0 \leftrightharpoons \mathrm{Si}_3^- + \mathrm{P}_4^+ . \tag{1}$$

This so-called autocompensation reaction takes into account that a negative Si_3^- dangling bond together with a positive, fourfold coordinated, substitutional P_4^+ donor is isoelectronic to a fourfold coordinated silicon Si_4^0 and a threefold coordinated neutral phosphorus atom P_3^0. In the employed notation, the lower index gives the coordination number and the upper index denotes the charge state of the respective atom. A similar relation holds for the case of p-type doping with boron:

$$\mathrm{Si}_4^0 + \mathrm{B}_3^0 \leftrightharpoons \mathrm{Si}_3^+ + \mathrm{B}_4^- . \tag{2}$$

The existence of boron acceptors B_4^- goes along with an increase of positively charged dangling bonds Si_3^+. However, experimentally, the energy levels of B and also of the resulting defect states have not been detected so far, thus remaining more uncertain than those of phosphorus.[11–15]

By means of Eqs. (1) and (2) the phenomena of substitutional doping in a-Si:H and the ensuing creation of charged defects in doped layers could be explained. A more refined view of doping in hydrogenated amorphous silicon has been developed subsequently in the context of the so-called defect-pool model which is also able to account for the increased density of charged dangling bonds in doped amorphous semiconductors.[16–19]

Substitutional doping in amorphous semiconductors has only been observed in the case of overconstrained networks

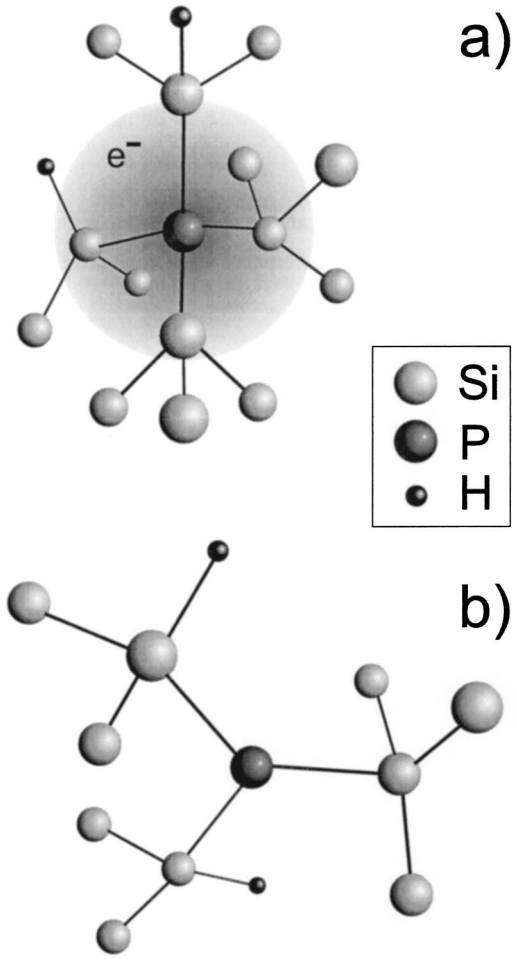

FIG. 1. Schematic models for electronically active (a) and inactive dopant configurations (b) for the case of phosphorus in amorphous silicon.

with an average fourfold coordination, i.e. for *a*-Si:H, *a*-Ge:H, *a*-C:H, their alloys, and furthermore for chalcogenide glasses with rather high concentrations of metal dopants (Ref. 20, and references therein). In amorphous hydrogenated silicon suboxides (*a*-SiO_x:H), $\langle r \rangle$ is decreased from the value of 4 towards lower average coordination by alloying with oxygen up to concentrations of 50 at.%. Consequently, the network is softened by the two-valent oxygen and changes its character from an amorphous semiconductor towards a semiconducting glass. The aim of this work is to investigate structural changes in the network and the corresponding behavior of optical, electronic, and electrical properties, particularly the doping efficiency, in the transition region between an overconstrained and an increasingly constraintfree amorphous network.

II. EXPERIMENTAL

Amorphous hydrogenated silicon suboxides are deposited by plasma enhanced chemical vapor deposition (PECVD) from the source gases SiH_4, H_2, and CO_2. By varying the SiH_4/CO_2 gas flow ratio, oxygen concentrations between 0 and 50 at.% can be achieved, resulting in optical band gaps E_{04} between 1.9 and 3.0 eV. *n*- and *p*-type doping is realized by adding PH_3 (1 vol.% diluted in SiH_4) and B_2H_6 (1 and 2 vol.% diluted in SiH_4), respectively, to the deposition gases. Intrinsic, *n*- and *p*-type *a*-SiO_x:H layers (150–1000 nm thick) were deposited on Corning 7059 glass or quartz at a substrate temperature of 250°C. The oxygen contents were varied between 0 and 45 at.%. In some cases, the hydrogen in the samples was effused in a vacuum setup, using a linear heating rate of 20 K/min up to temperatures of 800 °C, however, avoiding crystallization. For electrical measurements, Cr/Au gap contacts (40 and 100 nm thick, respectively) were evaporated onto the samples. The alloy composition of the samples was determined by elastic recoil detection (ERD) (Ref. 21) and energy dispersive x-ray spectroscopy. The concentration of carbon and other undesired impurities was below 1 at.% for all investigated samples. All oxygen concentrations quoted in this paper—unless stated differently—refer to the ratio $[O]/([O]+[Si])$. The absorption coefficient α and the optical gap E_{04} were determined from photothermal deflection spectroscopy (PDS) (Ref. 22) and transmission measurements. The mechanical hardness was measured by nanoindentation.[23] The dark conductivity was determined as a function of temperature in the range 300–500 K.

The defect densities were obtained by electron paramagnetic resonance (EPR) and from the midgap absorption in the PDS spectra. EPR was also measured in the dark, under white light and with Ar ion laser illumination at 514 nm to investigate the charge state of the defects [light-induced electron paramagnetic resonance (LEPR), $T \approx 10$ K]. Spin dependent photoconductivity (SDPC) at $T \approx 10$ K was used to determine the influence of oxygen on the donor wave function from the hyperfine structure of the substitutional phosphorus donor. The EPR spectrometer was a commercial x-band Bruker spectrometer equipped with a helium-gas-flow cryostat and an optically accessible cavity. A very low microwave power was chosen at 10 K in order to avoid saturation.

III. STRUCTURAL AND MECHANICAL PROPERTIES

In the case of the overconstrained *a*-Si:H, the average atomic coordination $\langle r \rangle$ always has a value of $\langle r \rangle = 4$ or slightly lower, depending on the amount of monovalent hydrogen which reduces the coordination to a certain extent. In contrast, chalcogenide glasses consist of elements with different valencies v, such as S, Se, Te ($v=2$), As ($v=3$), or Ge ($v=4$). As a consequence, the coordination usually is lower and can be tuned over a wide range by changing the material composition. Thus, it has been found that at a critical value of $\langle r \rangle = 2.4$, a transition from a ''rigid'' to a ''floppy'' network occurs.[3–5] Such a universal threshold at roughly 2.4 can be found for a variety of physical properties in many network glasses (Refs. 24, 25, and references therein).

This phenomenon can be explained as the percolation of rigidity through an amorphous network for $\langle r \rangle$ greater than 2.4. It is a consequence of the constraints, which increasing fractions of 3- or 4-valent elements introduce. Döhler[26] and Thorpe[27,28] have shown that the percolation threshold r_p

$=2.4$ can be calculated by counting the number of the so-called zero-frequency or floppy modes per atom, $f=F/N$, which allows one to continuously deform the network at no cost in energy:

$$f=\frac{F}{N}=3-\sum_i c_i\left[\frac{v_i}{2}+(2v_i-3)\right]. \quad (3)$$

Basically, the number of constraints introduced by the different network elements (N atoms, valencies v_i, and concentrations c_i) is counted and subtracted from the $3N$ degrees of freedom. Thus, $f=F/N$ gives the number of degrees of freedom per atom remaining in excess of the existing constraints. The first term $v_i/2$ in the sum of Eq. (3) takes into account the bond constraints whereas the second term $(2v_i-3)$ stands for the number of angular constraints.[27] r_p can then be determined as the value of $\langle r\rangle$ where f equals zero, i.e., where all internal degrees of freedom are compensated by the constraints. Since f can never become negative a theoretical hardness index $h=-f$ is defined for values $\langle r\rangle$ greater than the percolation threshold r_p. It characterizes the overconstrainedness of the material.[29] Thus, for the silicon-oxygen alloys studied in this work, the hardness index is the relevant quantity: Only stoichiometric SiO_2 with $\langle r\rangle\approx 2.65$ reaches a value close to the percolation threshold, whereas silicon itself and also SiO_x have mean coordinations larger than r_p.

In the following, these concepts will be applied to the case of a-SiO_x:H, with oxygen contents between 0 and 50 at. %. Structural features such as SiO_2 or Si clusters, silicon dangling bonds, molecular hydrogen inclusions, or microvoids with hydrogen terminated internal surfaces are likely to exist in the our samples. All these possible local configurations can have an influence on the network flexibility or rigidity and introduce complications in a simple effective-medium description of the structural and mechanical properties of a-SiO_x:H. The two major modifications, which have to be made for the calculation of $\langle r\rangle$ and f, arise from the presence of the monovalent hydrogen and the electronegative oxygen atoms.

First, silicon suboxides contain a significant fraction of hydrogen. Figure 2 shows the hydrogen content as a function of oxygen content for the investigated intrinsic, n-, and p-type SiO_x samples. In the case of a-Si:H ([O]=0), the hydrogen content is roughly 12–14 at. %. [H] increases similarly for doped and undoped silicon suboxides with rising oxygen content and reaches values around 20 at. % for [O] $\gtrsim$30 at. %. The scattering of the [H] values around 20 at. % becomes quite large for higher oxygen contents, which is due to increased plasma fluctuations at high deposition power. Presumably, the larger hydrogen fraction at higher [O] arises from the fact that Si—H bonds are stabilized by back-bonded oxygen atoms and, thus, more hydrogen is incorporated with increasing [O]. From these considerations, it is clear that hydrogen will make a noticeable contribution to $\langle r\rangle$ and f, which, according to Fig. 2, is expected to be more pronounced for larger oxygen contents.

However, it is a nontrivial problem, how singly coordinated atoms such as hydrogen contribute to the network

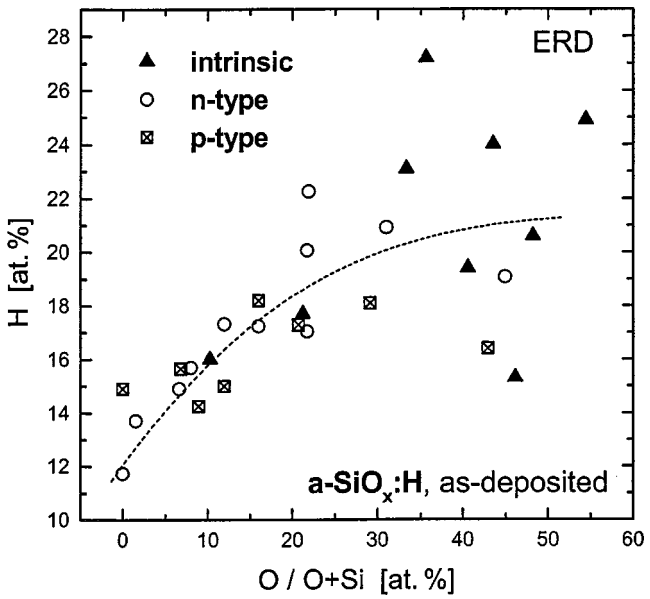

FIG. 2. Hydrogen content in intrinsic, n- and p-type a-SiO_x:H as a function of oxygen content ([O]/([O]+[Si])). The line is a guide to the eye.

properties.[24,25,29,30] Generally, monovalent hydrogen weakens the overconstrained network due to the fact that it passivates dangling bonds, which otherwise would form connections with other network atoms. One approach to calculate $\langle r\rangle$ is summing up the valencies v_i of Si (4), O (2), and H (1) weighted with their respective concentrations c_i,[24,29] as shown in Eq. (4):

$$\langle r\rangle=4\times c_{\mathrm{Si}}+2\times c_{\mathrm{O}}+1\times c_{\mathrm{H}},\ \textit{complete network}. \quad (4)$$

Another way of evaluating the average coordination is the so-called ''plucked network'' model (Ref. 29 and references therein). It takes into account that onefold coordinated atoms are percolatively ineffective and merely reduce the valency of the atom they bond to by one. In the case of a-SiO_x:H, the so-called ''complete network'' approach neglects the experimental fact that hydrogen preferentially bonds to silicon. Within the sensitivity of IR spectroscopy no evidence for the existence of O—H bonds in a-SiO_x:H was found. The existence of smaller numbers of O—H bonds cannot be entirely excluded for larger oxygen and hydrogen content (cf. Fig. 2), however, is unlikely to be an important issue. Thus, for the plucked network it is assumed that every H atom bonding to one Si atom reduces the valency of the respective Si atom from 4 to 3. Thus one has to consider two-valent oxygen, three- and four-valent silicon in order to determine $\langle r\rangle$ [Eq. (5)]:

$$\langle r\rangle=\frac{4\times c_{\mathrm{Si}}-1\times c_{\mathrm{H}}+2\times c_{\mathrm{O}}}{c_{\mathrm{Si}}+c_{\mathrm{O}}},\ \textit{plucked network}. \quad (5)$$

For both models, the presence of onefold coordinated atoms results in a softening of the network and a reduction of its mechanical hardness. The values of the plucked network were found to overestimate experimental results which, how-

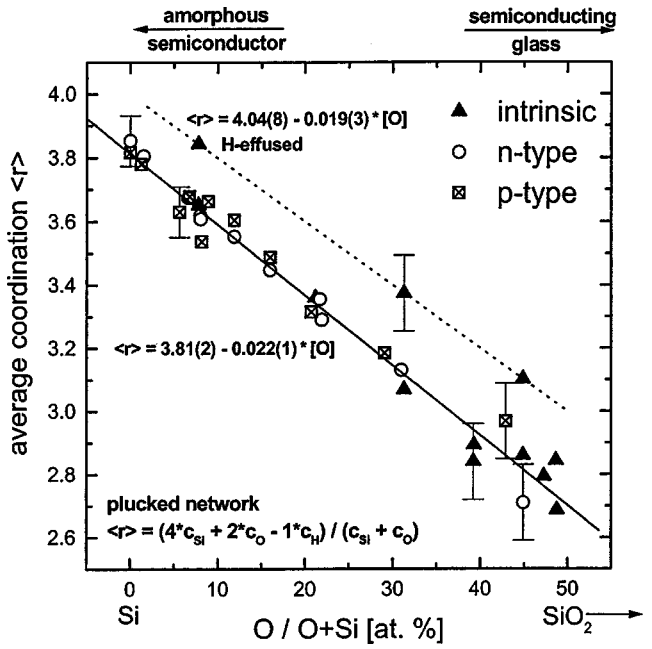

FIG. 3. Average coordination of intrinsic, *n*-, and *p*-type a-SiO_x:H, calculated according to the plucked network model. Data for a set of intrinsic hydrogen-effused samples are shown as well. The straight lines represent least-square fits to the data. Error bars are given exemplarily for some of the data points.

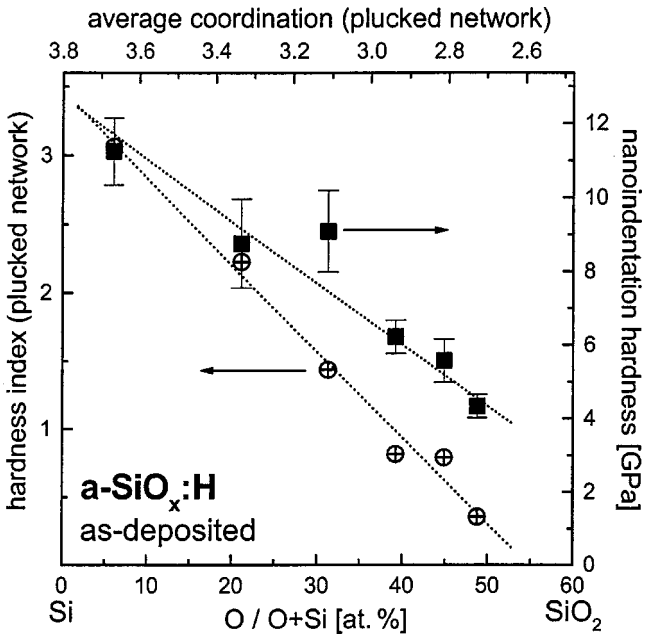

FIG. 4. Theoretical hardness index h (calculated for the plucked network) and mechanical hardness NIH as obtained from nanoindentation measurements as a function of oxygen content and average coordination for as-deposited, intrinsic a-SiO_x:H samples. The dotted lines are guides to the eye.

ever, is only a minor quantitative and never a qualitative effect in the case of silicon suboxides.[29] Nevertheless, for SiO_x the plucked network readily takes into account the preferential bonding of H to Si. Thus, for this work, the quantities $\langle r \rangle$, f, and h are defined in the framework of the plucked network model.

A second modification has to be made because of the electronegative oxygen atoms. Due to the polarizability of oxygen atoms, the Si—O—Si bond angle in SiO_2 is known to deviate significantly from 180° (Refs. 31,32) and the angular constraint associated with O is greatly relaxed. Thus, no angular constraint should be taken into account for the case of oxygen atoms.[26,27] Further corrections for other configurations, such as floppy inclusions within a rigid structure or the formation of ring structures, require a more refined theory[26–28] and experimental knowledge of a-SiO_x:H and have therefore not been considered for this analysis.

The average coordination of the "plucked" a-SiO_x:H network (doped and undoped samples), as obtained by ERD measurements, is shown in Fig. 3 as a function of oxygen content. For a-Si:H, $\langle r \rangle$ is roughly 3.8. The fact that this value is smaller than 4 can be explained by the influence of the Si−H bonds. With increasing [O], $\langle r \rangle$ decreases linearly and reaches a value of 2.7 for 50 at. %. This is still above the expected percolation threshold, but indicates that the material is getting less constrained and more flexible by adding oxygen. An extrapolation to [O]=66 at. % suggests that the average coordination decreases to approximately $\langle r \rangle \approx 2.4$. This value, however, is not identical to the percolation threshold for a-SiO_x:H, since r_p is determined from $f=0$ or $h=0$ and additionally depends on the respective hydrogen concentration. Thus, by varying the oxygen concentration, $\langle r \rangle$ can be tuned over a wide range, changing the a-SiO_x:H network from an amorphous semiconductor to a semiconducting glass.

Also shown for comparison is the average coordination of a set of samples, from which all hydrogen was effused. Without H, the values of $\langle r \rangle$ are roughly 0.2–0.3 larger than those in the samples with hydrogen, so that for pure a-Si, a value of 4 is indeed obtained at [O]=0. The relation $\langle r \rangle = 4.04 - 0.019 \times [\mathrm{O}]$ for samples without hydrogen leads to a higher value of $\langle r \rangle \approx 2.65$ at [O]=66 at. %, which is in good agreement with calculations for SiO_2 ($r_p \approx 2.65$) taking into account the relaxation of the oxygen angular constraint.[26,27]

According to Eq. (3) and with the mentioned modifications required for oxygen and hydrogen, the hardness index $h=-f$ can be calculated. Figure 4 compares the mechanical hardness of SiO_x:H determined by nanoindentation (NIH) and the expected hardness index h calculated from the composition data obtained by ERD. It shows these quantities for as-grown, intrinsic a-SiO_x:H samples. Both curves decrease with rising [O] and decreasing $\langle r \rangle$, respectively. The nanoindentation hardness for the sample with the lowest oxygen concentration is ≈11 GPa. This is comparable to values of NIH of ≈10 GPa, known for crystalline silicon[33,34] and amorphous silicon with [H]≤1 at. % (Refs. 34,35). However, Jiang *et al.*[34,35] and Hayes *et al.*[36] discovered that NIH of a-Si:H is reduced by approximately a factor of two upon adding up to 17 at. % hydrogen. These findings cannot be confirmed for our sample with 6 at. % [O] (NIH≈11 GPa) which contains 12 at. % hydrogen. One explanation might be that their samples were prepared by rf sputtering, whereas

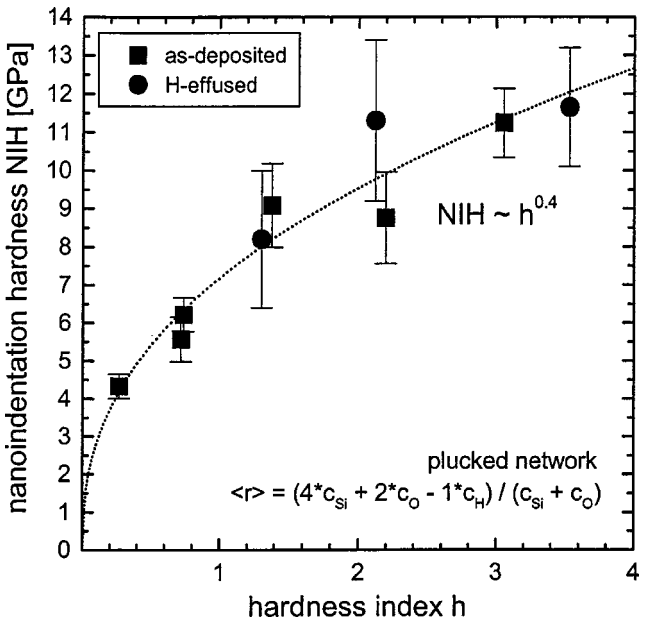

FIG. 5. Nanoindentation hardness vs calculated hardness index (plucked network) for as-deposited and H-effused samples. The line is a power-law fit to the data.

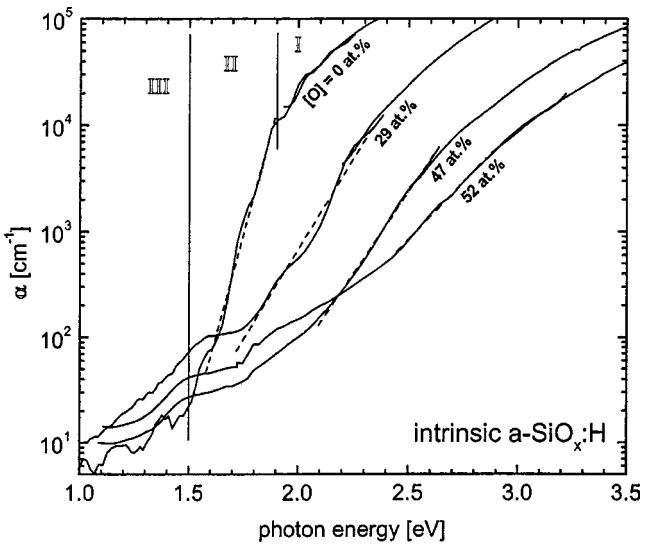

FIG. 6. Absorption spectra of intrinsic a-SiO_x:H with different oxygen contents of 0, 29, 47, and 52 at. %. The spectral regions of band-to-band (I), band tail (II), and defect absorption (III) are indicated for the sample without oxygen (a-Si:H). Straight dashed lines are fitted to the band tails to determine the Urbach energy E_0.

ours were deposited by PECVD. The different preparation techniques might account for the differences in the mechanical properties at large hydrogen contents. For increasing [O] up to 50 at. %, when the network is already substantially softened, but $\langle r\rangle \approx 2.8$ is still above the percolation threshold, NIH decreases towards 4 GPa. In contrast, the theoretical calculations for the hardness index h intersect with the x-axis already at 55 at. % oxygen and suggest a percolation threshold r_p for a-SiO_x:H of roughly 2.6 which again is quite similar to the value of $r_p \approx 2.65$ obtained for pure quartz.[26,27] This is an indication that the presence of $\approx$20 at. % hydrogen for $[O] \gtrsim 40$ at. % (cf. Fig. 2) shifts the percolation threshold to oxygen concentrations below 66 at. %. However, a more quantitative analysis is difficult since the complete omission of the oxygen angular constraint might be too drastic or corrections for ring formations or floppy inclusions ought to be considered. The fact that the experimental hardness values NIH do not tend towards zero in a similar way as the theoretical hardness h, with increasing [O] might be due to compositional inhomogeneities in the SiO_x samples such as cluster formation or phase separation. Also, a stabilization of the thin film by the underlying substrate might be an additional contribution.

The correlation between measured NIH and calculated hardness index is displayed in Fig. 5 for as-deposited as well as H-effused intrinsic SiO_x samples. Both sets of samples approximately follow the same relation. The nanoindentation hardness increases sublinearly with $\mathrm{NIH} \propto h^{0.4}$. However, it is difficult to speculate whether NIH indeed would decrease towards zero at $h=0$, as suggested by the fit to the data (dotted line). In contrast, Boolchand *et al.* found a linear correlation for thin films of diamondlike carbon.[29] Since not much systematic work exists on the mechanical properties of a-Si:H and its alloys with oxygen, the exact origin of this sublinear behavior remains unclear. The presence of three different atomic species (Si, O, H) in comparable fractions obviously makes an explanation complicated for a-SiO_x:H. For a more detailed understanding, effects such as clustering, phase separation, ring formation, or flexible inclusions have to be taken into account. Nevertheless, a good qualitative correlation between structural and mechanical properties of silicon suboxides has been shown for a wide range of oxygen contents. In the following sections, it is investigated how the decrease in mean coordination upon alloying with increasing amounts of oxygen affects electronic, optical, and electrical properties of a-SiO_x:H, especially the doping efficiency of n- and p-type doped samples.

IV. ELECTRONIC AND OPTICAL PROPERTIES

The changes in structure with increasing [O] also give rise to significant modifications of the electronic density of states in silicon suboxides. Figure 6 shows the absorption spectra of intrinsic a-SiO_x:H for four different oxygen contents (0, 29, 47, and 52 at. %). For the a-Si:H sample ($[O]=0$), three characteristic regions of absorption are indicated. Region I corresponds to band-to-band absorption, region II originates from absorption processes involving band tail states, and region III arises from absorption via Si dangling bond defect states in the middle of the band-gap. These regions are also discernible for the other curves, which, however, become less distinguishable with rising oxygen concentration. The value of the band-gap E_{04} increases from approximately 1.9 to 3.0 eV for [O] between 0 and 50 at. %. The band tails (II) of our SiO_x samples start out with an Urbach energy of about 70 meV for a-Si:H, broaden significantly with rising oxygen content, and reach a value of roughly 200 meV for 50 at. % oxygen. Also, the defect absorption changes with increasing oxygen content. In the energy region between 1.0 and 1.5 eV,

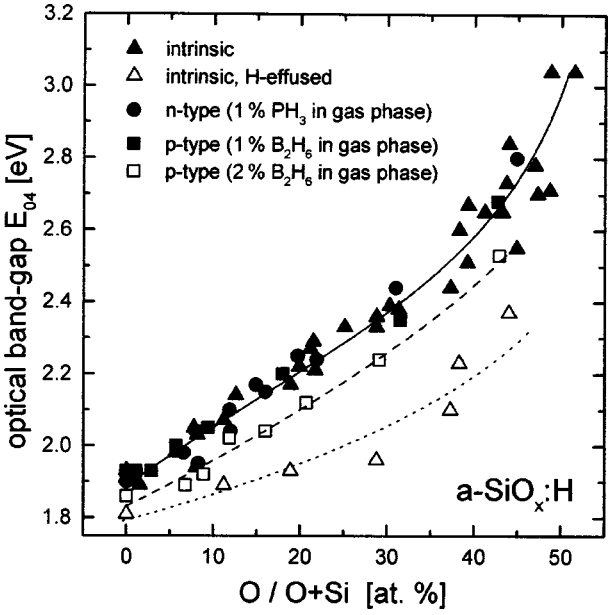

FIG. 7. Optical band-gap E_{04} of intrinsic (as deposited and H effused), *p*-type (1% and 2% B_2H_6 in the gas phase), and *n*-type silicon suboxides (1% PH_3 in the gas phase) as a function of oxygen content. The lines are guides to the eye.

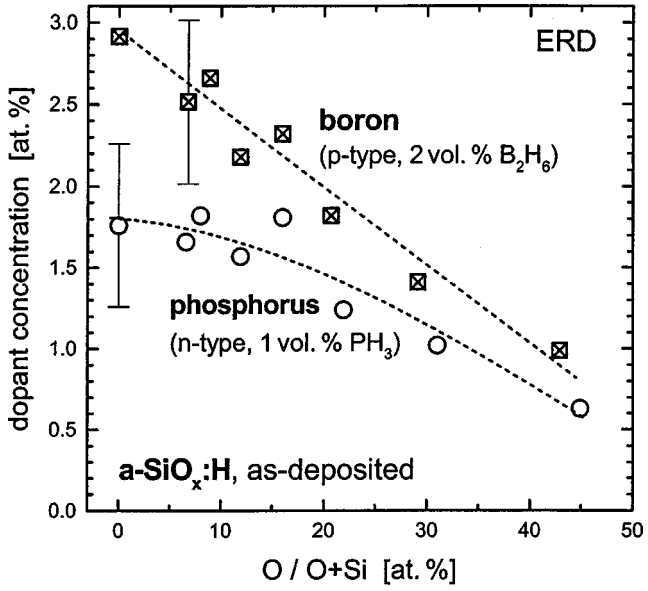

FIG. 8. Phosphorus and boron solid-phase concentrations of *n*- and *p*-type a-SiO_x:H (1% PH_3 and 2% B_2H_6 in the gas phase), respectively, as a function of the oxygen content [O]/([O]+[Si]). The lines are guides to the eye.

the sample without oxygen possesses the lowest defect absorption. The incorporation of oxygen creates additional defects and accordingly increases α. Defect densities can be calculated from subgap absorption using a calibration procedure described elsewhere.[32,37] However, this calibration is not trivial because with increasing oxygen content the optical gap and also the region of defect absorption shift in energy. Therefore, the uncertainty in the deduced absolute defect concentrations N_D is approximately a factor of two, whereas the relative errors between samples are much smaller. Note that our samples with [O]=0 at. % have higher Urbach energies and defect densities than optimized state-of-the-art a-Si:H samples because of residual oxygen contamination and nonoptimized deposition conditions for pure amorphous silicon.

The dependence of the optical band-gap E_{04} on the oxygen concentration is shown in more detail in Fig. 7 for different sets of samples. For the as-deposited intrinsic and the doped SiO_x samples with 1% dopant concentration in the gas phase, the increase of the band gap is similar for all [O]. Up to roughly 40 at. %, E_{04} displays a slow linear increase from 1.9 to roughly 2.6 eV. This corresponds to oxygen contents where the conduction band (CB) and valence band (VB) are still dominated by Si—Si bonds. Above 40 at. % oxygen, these Si—Si bonds are gradually replaced by oxygen lone pairs (VB) and Si—O bonds (CB), causing a more rapid increase of the band-gap ($\approx$3 eV at 50 at. %).[38,39] Generally, the observed behavior of the optical gap agrees well with the results shown in previous publications.[40–43] However, E_{04} was found to depend on the deposition technique and the resulting hydrogen content of the samples. For H-effused samples (open triangles), E_{04} also shows an increase with [O], but the values are lower than those for the samples with H and rather compare to sputtered a-SiO_x samples with a very low hydrogen concentration.[44] During the outdiffusion of hydrogen, Si—H bonds are gradually replaced by dangling bonds and the defect density increases. Also, weak Si—Si bonds situated at the band edges are restored, which leads to a shift of the band edges into the band-gap and correspondingly to the lowering of E_{04} by $\approx$0.1–0.4 eV displayed in Fig. 7. Also the *p*-type samples with a higher gas-phase dopant level of 2% B_2H_6 exhibit $\approx$0.1 eV lower values of E_{04} (open squares). In this case, however, it is not due to a lower hydrogen content of the *p*-type samples (see Fig. 2). Rather, additional states introduced by the larger boron concentration[13–15] or changes of the deposition conditions are likely to account for the reduced optical gaps. As Fig. 7 shows, the optical band-gap can vary quite significantly even for the same oxygen content. Therefore, the investigated physical quantities have to be plotted as a function of a parameter which includes variations not only of the oxygen concentration but also of the hydrogen content and the deposition technique. In contrast to the oxygen content, the optical gap E_{04} is such a general quantity depending on [O], [H], and the preparation conditions. To ensure a meaningful comparison between the different series of samples most of the data will therefore be displayed as a function of E_{04} in the following sections, especially when dealing with transport properties.

With our current PECVD setup only *p*-type suboxides with a B_2H_6 gas-phase concentration of 2% can be manufactured in contrast to *n*-type samples with 1% PH_3. However, the solid-phase concentrations of phosphorus and boron (Fig. 8, determined by ERD), show a more complicated behavior: For *p*-type samples, the boron concentration is almost 3 at. % for the a-Si:H sample ([O]=0). With rising oxygen concentration, [B] decreases linearly and reaches a value of 1 at. % at the highest [O]. For phosphorus, in contrast, the

concentration is ≈ 1.5–2 at. % for [O] $\lesssim 20$ at. %. Only for higher oxygen fractions the *P* concentrations start to decrease in a similar way as for the boron-doped samples. Especially for larger oxygen contents (>10 at. %) the differences between *n*- and *p*-type samples are smaller than those suggested by the gas-phase concentrations. Apparently, the incorporation efficiency of boron atoms cannot be increased in the same way as the diborane concentration. Also, it can be seen that a sufficiently large dopant incorporation (roughly 1 at. %) is possible even at high oxygen contents so that a meaningful investigation of the doping efficiency can be performed. The comparable solid-phase dopant concentrations justify the comparison of *n*- and *p*-type SiO_x despite initially different gas-phase concentrations. In addition, the conductivity data of Fig. (11) will show that there are only insignificant differences between samples with 1% (earlier data) and 2% B_2H_6 if plotted as a function of the optical band-gap.

In addition to alloying with increasing oxygen fractions, dopant incorporation also produces significant changes in the absorption of *n*- and *p*-type a-SiO_x:H samples compared to intrinsic samples. In Fig. 9 the absorption coefficients α of *n*- [part (a)] and *p*-type [part (b)] amorphous silicon suboxides for oxygen contents between 0 and 45 at. % are displayed. The E_{04} values have already been discussed in the context of Fig. 7. In contrast to undoped samples (Fig. 6), the subgap absorption is significantly higher in doped SiO_x, in particular for the lower oxygen contents. The boundary between band tail and defect absorption is difficult to recognize for almost all of the curves shown. For pure a-Si:H, the increase in subgap absorption can be explained by the doping-induced generation of charged defects according to the autocompensation reaction [Eqs. (1) and (2)]. This situation changes upon alloying with increasing oxygen concentration: The larger the oxygen concentration, the lower is the doping-induced increase of the subgap absorption. As a consequence, the subgap absorption at a given photon energy decreases by roughly one order of magnitude from 0 to 45 at. %, both for *n*- and *p*-type samples. The defect absorption α_D is slightly stronger for boron-doped a-SiO_x:H and its reduction is less pronounced, which can be understood from the higher concentration of 2% B_2H_6 in the gas phase. Note that this decrease of the subgap absorption in doped SiO_x is the opposite of what is observed in intrinsic samples. Here, the defect absorption successively increases by about one order of magnitude when [O] increases from 0 to 45 at. % (see Fig. 6). Indeed, for large oxygen concentrations, the values of α_D for doped and undoped samples become comparable, which will be discussed in more detail in the following section.

Figure 10 shows the behavior of the dark conductivity σ_D of doped a-SiO_x:H with increasing oxygen content. σ_D is plotted as a function of the inverse temperature for *n*- [part (a)] and *p*-type $a-SiO_x$ [part (b)]. The increase of [O] and E_{04}, respectively, results in a drastic decrease of the dark conductivities over several orders of magnitude for both types of samples. In the case of *n*-type SiO_x, the drop of the room-temperature dark conductivity comprises more than ten orders of magnitude. Boron doping is less effective[45] and the decrease of $\sigma_{D,p}$ (roughly 6–7 orders of magnitude) is not as pronounced as in the case of $\sigma_{D,n}$.

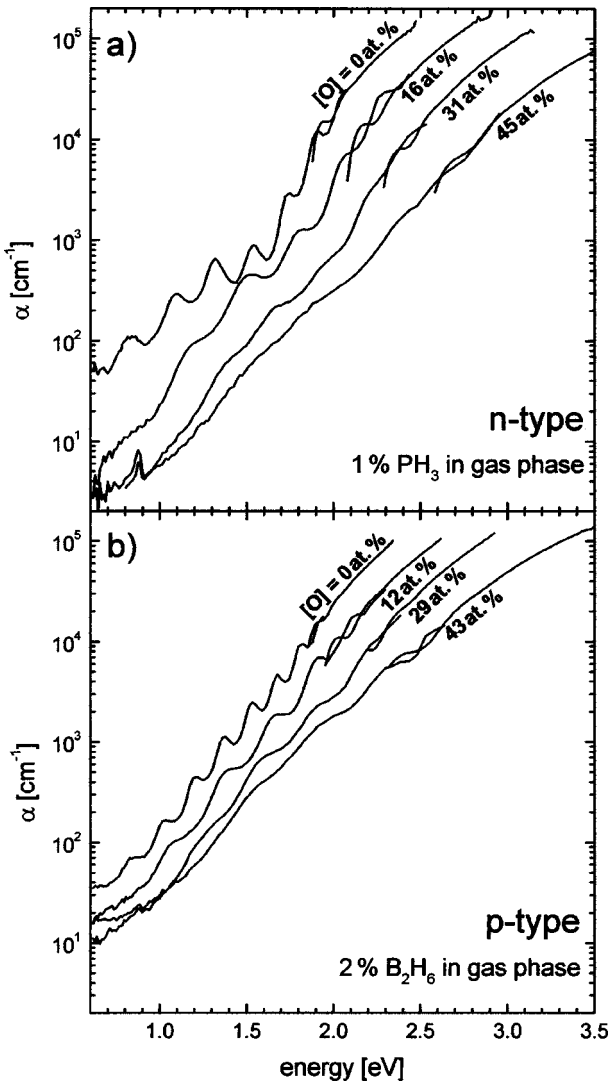

FIG. 9. Absorption spectra of *n*-type (a) and *p*-type (b) a-SiO_x:H with oxygen contents between 0 and 45 at. %. The gas-phase dopant levels were 1% PH_3 for P-doped and 2% B_2H_6 for B-doped samples.

Figure 11 contains a compilation of the room-temperature dark conductivities [part (a)] and the activation energies E_a [part (b), derived from the temperature dependence of σ_D] for intrinsic, *n*-, and *p*-type amorphous silicon suboxides as a function of the optical gap E_{04}. It allows one to distinguish between the effects which are produced by dopant incorporation and the changes caused by alloying with increasing oxygen concentrations. In Fig. 11(a), the *n*-type conductivity for $E_{04}=1.9$ eV (a-Si:H) is more than three orders of magnitude higher ($\sigma_{D,n}\approx 10^{-2}\,\Omega^{-1}\,\mathrm{cm}^{-1}$) than the *p*-type conductivity ($\sigma_{D,p}\approx 10^{-5}\,\Omega^{-1}\,\mathrm{cm}^{-1}$), which in turn is four orders of magnitude larger than the intrinsic one ($\sigma_{D,i}\approx 10^{-9}\,\Omega^{-1}\,\mathrm{cm}^{-1}$). These results agree qualitatively with previous data for a-Si:H.[45] As already shown in Fig. 10 all conductivities decrease with increasing band gap. Over the

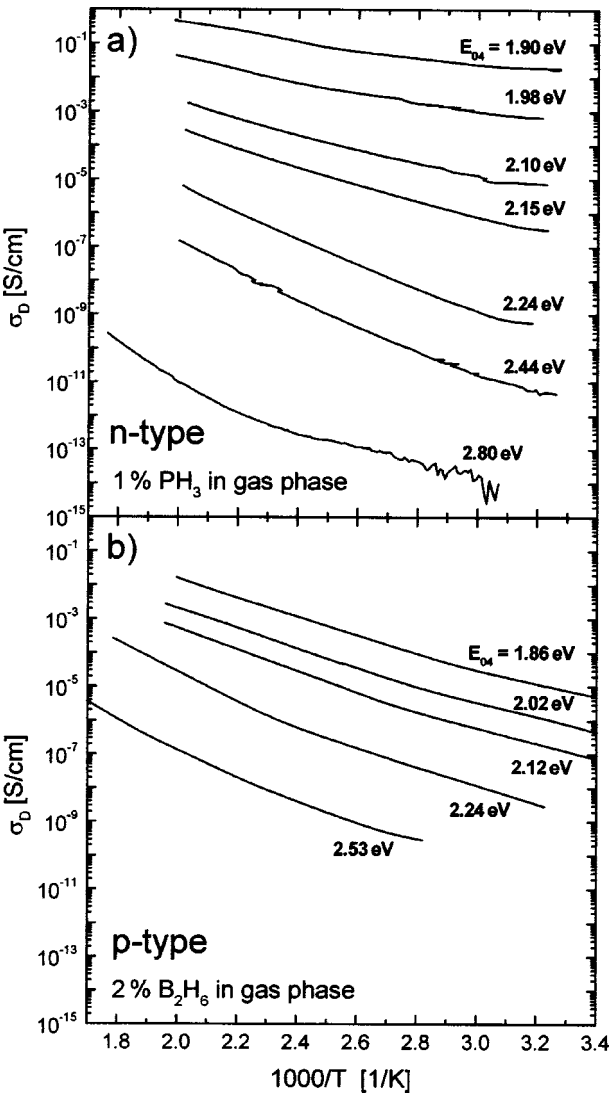

FIG. 10. Dependence of the dark conductivity σ_D of *n*- (a) and *p*-type (b) $a-SiO_x$:H on inverse temperature. The gas-phase dopant levels were 1% PH_3 for P-doped and 2% B_2H_6 for B-doped samples. The optical band-gaps E_{04} were in the range of 1.90–2.80 eV for *n*-type and 1.86–2.53 eV for *p*-type silicon suboxides. (See Fig. 7 for the corresponding oxygen concentrations.)

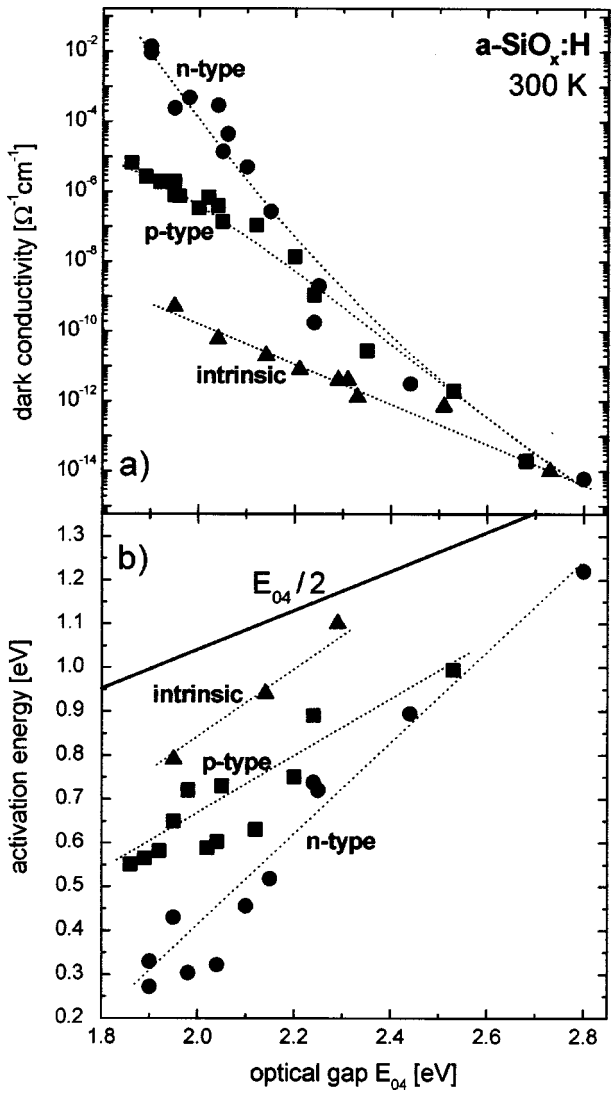

FIG. 11. Room-temperature dark conductivities (a) and activation energies (b) of intrinsic, *n*-, and *p*-type a-SiO_x:H as a function of the optical gap E_{04}. The gas-phase dopant concentrations were 1% for PH_3 and 1% and 2% for B_2H_6. The position of the middle of the band-gap $E_{04}/2$ is indicated by a thick solid line in part (b). The other lines are guides to the eye.

entire range of oxygen concentrations, the decline comprises 12 orders of magnitude for *n*-type (1 % PH_3), 9 for *p*-type (1 and 2 % B_2H_6), and only 5 for intrinsic samples. Although *p*-type silicon suboxides with two different gas-phase boron concentrations were examined, the dark conductivities of these samples are very similar if plotted as a function of the optical gap E_{04}. Thus, in spite of a larger gas-phase B_2H_6 concentration of 2 at. % the number of electrically active acceptors and the doping efficiency cannot be further enhanced. This similarity between the two sets of boron-doped samples allows us to compare either of them to the series of *n*-type suboxides. All conductivities—of doped and undoped SiO_x—converge towards a value of $10^{-14}\,\Omega^{-1}$ cm^{-1} for the highest E_{04} and [O], respectively. Experimentally, doping becomes inefficient at $E_{04}\approx 2.4$ eV ([O] ≈ 30 at. %), where all samples essentially show intrinsic character.

This can also be seen from the activation energies E_a [Fig. 11(b)], which were derived from the slopes of the Arrhenius plots in Fig. 10. E_a is the energy distance between E_F and the band edges and accounts well for the behavior of σ_D in Fig. 11(a). The activation energy is roughly 0.3 eV for *n*-type, 0.55 eV for *p*-type and 0.7–0.8 eV for our a-Si:H samples with $E_{04}\approx 1.9$ eV, indicating an efficient doping process at low oxygen contents. With rising E_{04}, E_a continuously increases for all samples up to values above 1 eV where E_F is located approximately in the middle of the optical gap. For the *n*-type case, E_a starts at 0.3 eV and increases up to 1.2 eV for the highest amount of oxygen. Thus, the Fermi level is shifted away from a position close to the conduction-band edge and is essentially pinned close to mid-

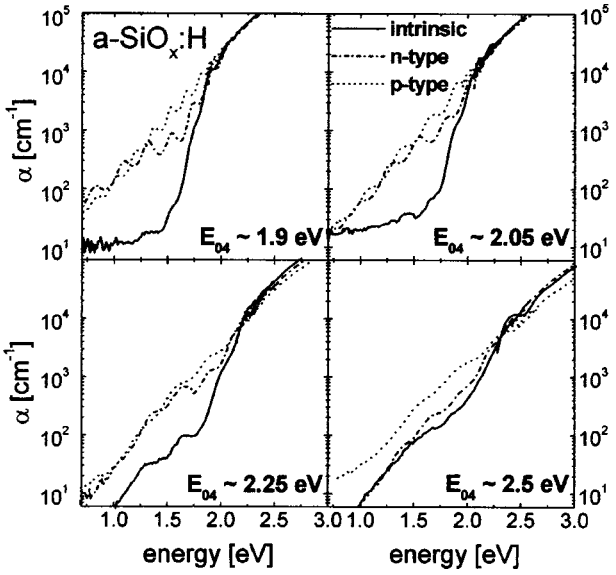

FIG. 12. Absorption coefficients α of intrinsic (solid lines), n-type (1% PH_3, dotted lines), and p-type (2% B_2H_6, dashed lines) a-SiO_x:H samples with optical gaps E_{04} of 1.9, 2.05, 2.25, and 2.5 eV.

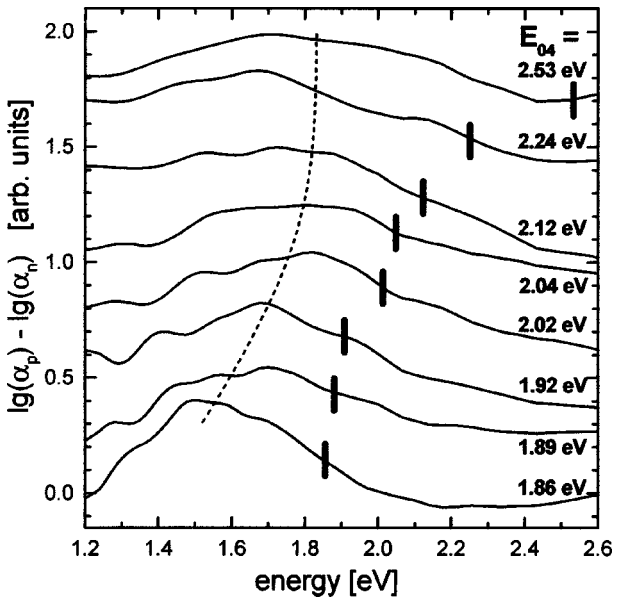

FIG. 13. Difference between the absorption spectra of p-and n-type a-SiO_x:H (2% B_2H_6 and 1% PH_3 in the gas phase, respectively) depicted by the quantity $\lg(\alpha_p)-\lg(\alpha_n)$. The dashed line indicating the approximate peak position is a guide to the eye. The values of the optical band-gap E_{04} ranging from 1.86 to 2.53 eV are also shown by vertical bars.

gap by the dangling bond defects for $E_{04}>2.4$ eV ([O] >30 at. %). A similar but weaker shift from $E_a=0.55$ eV to roughly 1.0 eV is also observed for p-type a-SiO_x ($E_{04}=1.85-2.53$ eV). As already observed for the dark conductivities, also the activation energies of n- and p-type samples approach each other above $E_{04}=2.4$ eV. Note that the activation energies of intrinsic suboxides are close to $E_{04}/2$ in all cases. However, the Fermi level is not exactly in the middle of the optical gap for undoped samples.

V. DEFECT DENSITIES

The transition from doped to intrinsic behavior with increasing oxygen content can also be seen from the defect absorption of doped and undoped silicon suboxides with similar band-gap. Figure 12 shows the absorption coefficient of intrinsic, n- and p-type SiO_x for four different optical band-gaps ($\approx$1.9, 2.05, 2.25, and 2.5 eV). Together with the shift of E_{04} from 1.9 to 2.5 eV, also the band tails broaden with increasing [O] for both doped and undoped samples. However, in the region between 1.0 and 2.0 eV where absorption occurs via defect states located in the middle of the gap, significant differences are observed. The defect absorption α_D is higher for both the phosphorus- and the boron-doped samples than for the intrinsic ones. At $E_{04}=1.9$ eV (0 at. % oxygen), the difference is almost two orders of magnitude. This difference is less pronounced for higher [O] and almost disappears at $E_{04}\gtrsim 2.4$ eV ([O]$\gtrsim$30 at. %), where the PDS spectra of doped and undoped SiO_x approach each other, again suggesting inefficient doping at higher oxygen contents.

A detailed comparison between the spectra of doped suboxides, however, reveals that the high-energy part of the defect absorption shoulder of p-type samples is always slightly larger than that of n-type samples (see Fig. 12). A closer analysis is shown in Fig. 13. The quantity $\lg(\alpha_p)-\lg(\alpha_n)$ represents the ratio of p- and n-type absorption raw data on a logarithmic scale and is calculated for optical gaps $E_{04}=1.86$–2.53 eV. The higher absorption of boron-doped samples results in a broad peak which extends over the subgap range from 1.2 eV up to values larger than E_{04} for all [O]. According to the increase of the optical band-gap as a function of [O] the position of this subgap peak gradually shifts from about 1.5 eV to roughly 1.8 eV . The peak energy is $\approx$0.2–0.7 eV smaller than E_{04}. The excess absorption strength of p-type material is equivalent to about 10^{19} cm^{-3} defects and also the energetic position of the broad absorption peak is similar or even higher than that of dangling bonds. Therefore, this p-type specific absorption might be an indication for a boron-related transition which does not exist or has a smaller transition matrix element for phosphorus in n-type material. For the p-type samples with 2% B_2H_6, these states account for the reduced band-gaps and their existence is also likely to prevent an enhancement of the doping efficiency despite a higher boron concentration. On the other hand, the B content in the p-type samples (2% B_2H_6) is somewhat larger in contrast to P in n-type SiO_x (cf. Fig. 8), a fact which might contribute to the described differences between n- and p-type absorption, as well.

The transition of P- or B-doped a-SiO_x:H towards increasingly intrinsic behavior with increasing [O] can be understood quantitatively by means of the respective defect densities from subgap absorption ($N_{D,Abs}$, see first paragraph of Sec. (IV) for details) and from EPR data ($N_{D,EPR}$). Figure 14 shows $N_{D,Abs}$ and $N_{D,EPR}$ for n-type [Fig. 14(a)] and p-type silicon suboxides [Fig. 14(b)] as a function of E_{04} and $\langle r\rangle$. In part (a) of Fig. 14, $N_{D,Abs}$ of n-type samples

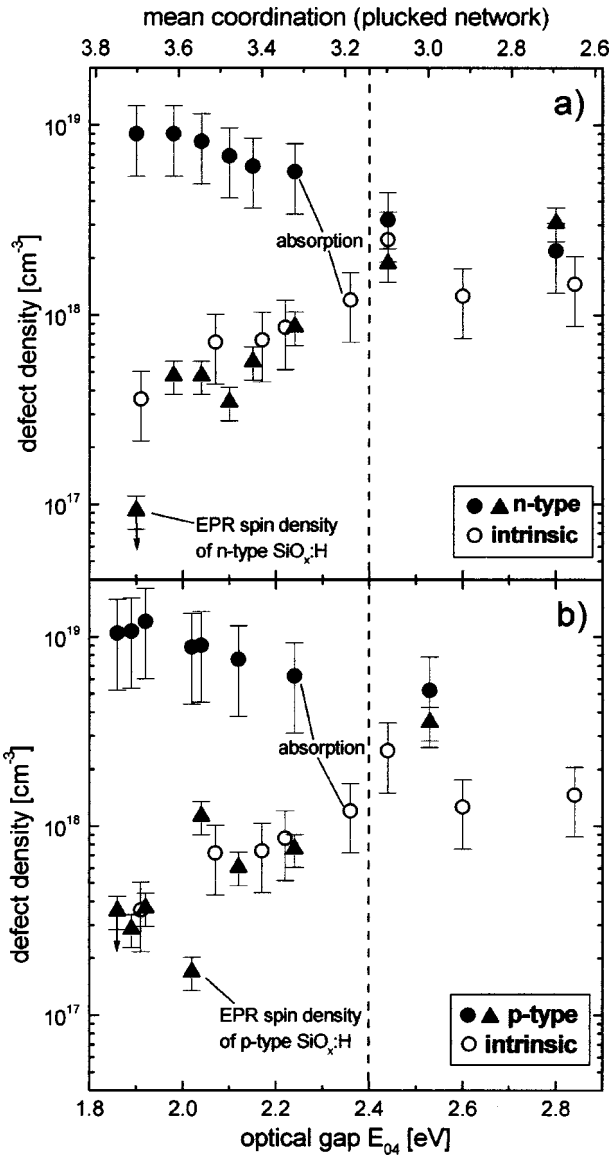

FIG. 14. Defect densities determined from absorption (solid circles) and EPR data (solid triangles) for *n*-type (a) and *p*-type a-SiO_x:H (b) as a function of optical band-gap E_{04} and average coordination $\langle r \rangle$. The gas-phase dopant levels were 1% PH_3 for P-doped and 2% B_2H_6 for B-doped samples. Also shown for comparison in both parts of the figure is the defect density of intrinsic a-SiO_x:H, as obtained from absorption measurements (open circles). The dashed line indicates the threshold at $E_{04} \approx 2.4$ eV ($[O] \approx 30$ at. %), above which doped material becomes intrinsic due to the failure of doping.

(solid circles) decreases with increasing E_{04} (1.9–2.8 eV) from 10^{19} cm^{-3} to $2\times10^{18} cm^{-3}$, whereas $N_{D,Abs}$ of intrinsic SiO_x (open circles, shown for comparison) increases from about 10^{17} cm^{-3} to 2×10^{18} cm^{-3}. Again, the difference is large at $E_{04}=1.9$ eV (0 at. % oxygen) and disappears above 2.4 eV ($[O] \approx 30$ at. %), where both values of $N_{D,Abs}$ are similar. In order to understand the origin of the different absorption behavior, the charge states of the defects in doped and undoped samples have to be considered. Equation (1) suggests that together with every active fourfold coordinated P_4^+ donor one negatively charged silicon dangling bond Si_3^- is created. Thus, the larger midgap absorption of *n*-type SiO_x for $E_{04}<2.4$ is likely to arise from these doping-induced Si_3^- states. In contrast, neutral dangling bonds should prevail in intrinsic a-SiO_x:H. They tend to increase with [O] and E_{04} according to rising disorder.

As PDS detects the absorption of dangling bond states irrespective of their charge, in addition EPR measurements were made, which are only sensitive to the neutral paramagnetic dangling bonds. For intrinsic SiO_x it has been confirmed that the defect absorption is due to neutral dangling bonds.[32] For *n*-type material with large concentrations of negative defects, the difference between PDS and EPR defect density is indeed large, as shown in Fig. 14(a) (solid circles and triangles). Furthermore, $N_{D,EPR}$ of *n*-type and $N_{D,Abs}$ of intrinsic SiO_x are comparable, i.e., the density of paramagnetic states is roughly the same in doped and undoped samples. This leads to the conclusion that in *n*-type material the excess defect density $N_{D,Abs}-N_{D,EPR}$ arises from the negatively charged dangling bonds created by phosphorus doping. At $E_{04} \approx 2.4$ eV ($[O] \approx 30$ at. %) where EPR and PDS defect densities become comparable, the prevailing defects must be neutral in spite of the presence of P.

A similar behavior of the defect densities is also detected for boron-doped *p*-type SiO_x (2% B_2H_6 in the gas phase) in Fig. 14(b). For $E_{04}=1.86$–2.53 eV, the overall defect density $N_{D,Abs}$ decreases from above 10^{19} cm^{-3} to roughly 5×10^{18} cm^{-3}, whereas $N_{D,EPR}$, which represents the fraction of paramagnetic states, increases from 3×10^{17} cm^{-3} to $(4-5)\times10^{18}$ cm^{-3}. As in *n*-type material, the excess density $N_{D,Abs}-N_{D,EPR}$ of charged defects, which now arises from positively charged dangling bonds Si_3^+ and indicates an efficient doping process, disappears above $E_{04} \approx 2.4$ eV ($[O] \approx 30$ at. %). Then, similar to phosphorus-doped material, the majority of the defects is neutral despite the boron incorporation and the doped suboxides possess intrinsic properties.

The behavior of the electronic g factors of the EPR resonances additionally supports the conclusions of Fig. 14. In accordance with the position of the Fermi level, it is known for a-Si:H that *n*-type material has a g factor of 2.0044 due to electrons in the conduction-band tail, boron-doped samples have g values of 2.008–2.013 due to holes in the valence-band tail, and the neutral Si dangling bond yields a signal at $g=2.0055$ for intrinsic samples.[11,46–49] In our case of a-SiO_x:H, a transition of the samples from doped to intrinsic occurs with increasing oxygen content and optical band-gap, respectively. Thus, depending on [O] and E_{04}, a mixture of contributions with different g factors is expected to exist in silicon suboxides. Due to the disordered nature of our a-SiO_x:H samples it is, however, impossible to deconvolute these contributions to the obtained EPR spectra. Therefore, only effective average g values g_{eff} are displayed in Fig. 15 as a function of E_{04} for undoped and doped samples. They are calculated from the center fields $H_{center} \propto {g_{eff}}^{-1}$ (see inset of Fig. 15) of the respective EPR resonances. In spite of the limitations which exist for such an interpretation (e.g., differences in passage conditions), the effective g-values can at least be regarded as an approximate

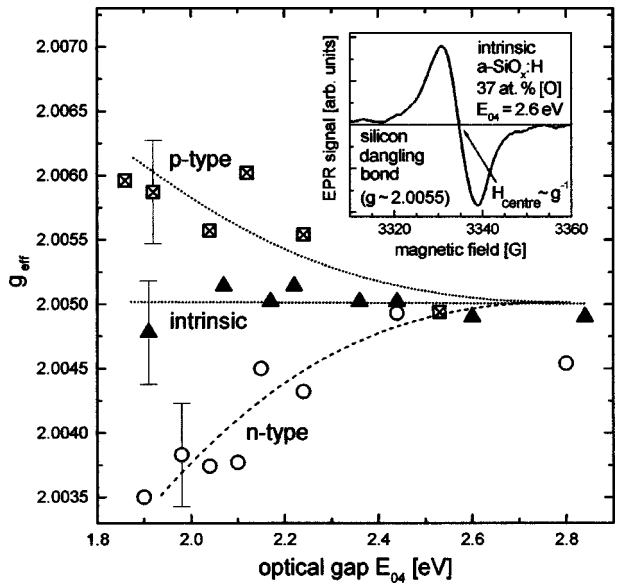

FIG. 15. Effective g factors g_{eff} ($\propto H_{center}^{-1}$) of the EPR resonances for intrinsic, n-type (1% PH_3), and p-type (2% B_2H_6) a-SiO_x:H samples as a function of the optical gap E_{04}. Exemplarily, the characteristic Si dangling bond EPR signal at $g \approx 2.0055$ for an undoped a-SiO_x:H sample with 37 at. % oxygen is shown in the inset. The dotted lines are guides to the eye.

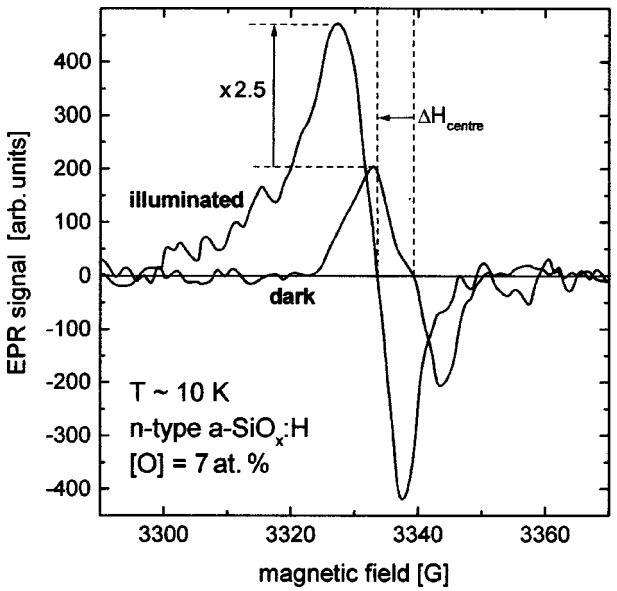

FIG. 16. EPR spectra of n-type a-SiO_x:H ([O]=7 at. %, 1% PH_3 in gas phase) at $T \approx 10$ K with and without illumination. The shift of H_{center} ($\propto g^{-1}$) and the increase of the amplitude are indicated.

measure for the position of the Fermi level in the optical band-gap and permit a qualitative comparison to a-Si:H. For intrinsic SiO_x, g_{eff} exhibits an approximately constant value of 2.0050 for all E_{04}.[32] For n-type SiO_x, g_{eff} is roughly 2.0035 at $E_{04}=1.9$ eV, increases monotonously and converges with the intrinsic g values of ≈ 2.0050 for $E_{04} \geqslant 2.4$ eV ([O]$\geqslant$30 at. %). A similar but opposite behavior is observed for p-type samples. Here, g_{eff} at 1.86 eV is about 2.0060 and also converges with the values of n-type and intrinsic samples at 2.4 eV. These shifts of the effective g factors of doped samples towards the intrinsic values confirm the movement of the Fermi level towards the middle of the band-gap and the inefficient doping for increasing oxygen content.

For the case of phosphorus doping, the presence of a majority of Si_3^- states (negatively charged dangling bonds) can be shown by illumination of the n-type samples with low oxygen contents with white or laser light at low temperatures. Figure 16 shows the EPR spectra of n-type a-SiO_x:H ([O]=7 at. %) without and with illumination. In the dark, the effective g factor is roughly 2.0035 and the electrons in the conduction-band tail only produce a weak signal amplitude. Upon illumination, the generated holes are predominantly captured by the negative dangling bonds, which can be detected by a light-induced increase of the EPR intensity by a factor of ≈ 2.5 and a corresponding shift of the center field by several Gauss towards higher values of $g \approx 2.0065$. A summary of the effects of illumination on the EPR spectra of n-type a-SiO_x:H is given in Fig. 17 as a function of E_{04}. Without light, the EPR defect density in part (a) of Fig. 17 (solid circles) displays the increase with rising optical band-gap, which was already shown in Fig. 14(a). A very good agreement was observed for dark EPR data measured at 10 and 300 K. Strong illumination leads to a transformation of a significant fraction of the negative defects into neutral ones. This can be seen as a light-induced increase of $N_{D,EPR}$ (open circles) to a level of $(1-2)\times 10^{18}$ cm^{-3} for small values of $E_{04} \leqslant 2.2$ eV. The difference to the defect density in the unilluminated state is almost one order of magnitude at the lowest E_{04}, but decreases with rising band-gap and completely vanishes around 2.3–2.4 eV. Also, a significant shift of the effective g factors is observed upon illumination [Fig. 17(b)]. Again, the values of g_{eff} in the dark (solid circles) are comparable to those previously shown in Fig. 15. Under illumination, there is a distinct light-induced shift towards higher values of $g_{eff} \approx 2.006$–2.007 (open circles) for small E_{04}. This shift of g_{eff} is slightly larger than only to the intrinsic g factor of ≈ 2.0050 (cf. Fig. 15). Since the values of g_{eff} can be interpreted as an approximate indication for the position of the Fermi level or, in the case of light-induced EPR, the position of the quasi-Fermi levels,[50–52] holes trapped in the valence-band tails upon strong illumination might possibly shift the quasi-Fermi level for holes into the valence-band tail and, thus, be responsible for the additional shift of g_{eff} towards 2.006–2.007. Generally, the light-induced EPR spectra of P-doped SiO_x confirm the existence of large numbers of doping-induced negative dangling bonds at small oxygen contents. Similar arguments apply for p-type silicon suboxides.

VI. THE DOPING EFFICIENCY

For a quantitative analysis of the doping efficiency, the number of electronically active dopant atoms in the SiO_x matrix has to be determined. Initially, extended x-ray absorption fine structure[53] and nuclear-magnetic-resonance

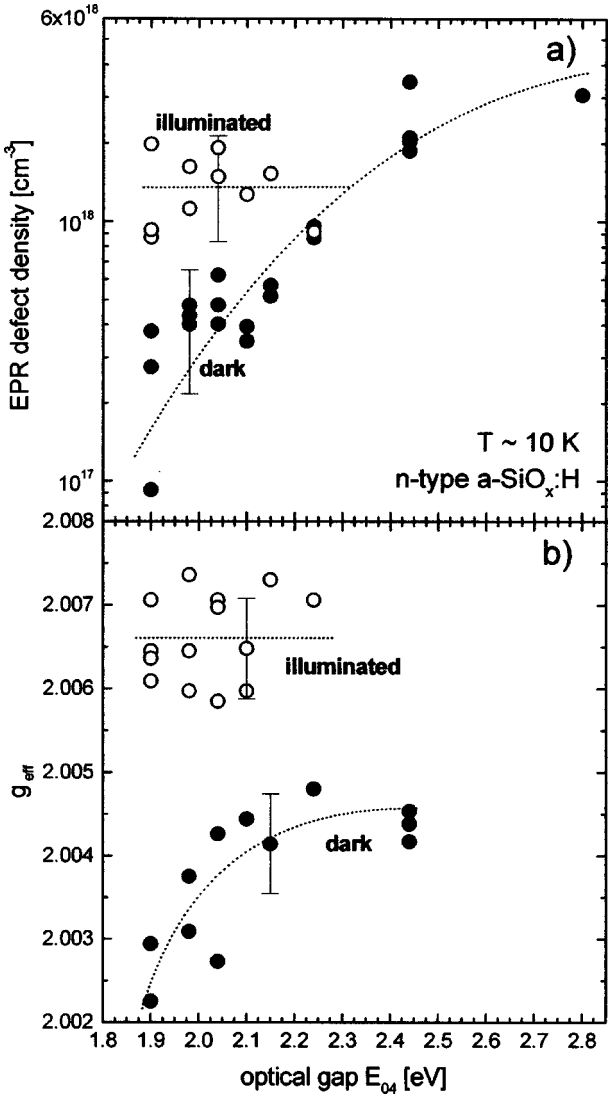

FIG. 17. Defect densities $N_{D,EPR}$ (a) and effective g factors g_{eff} of the EPR resonance (b) of n-type SiO_x samples (1% PH_3) as a function of the optical gap E_{04}. The samples were measured at $T \approx 10$ K in the dark and under white light and Ar ion laser illumination. The dotted lines are guides to the eye.

experiments[54–57] attempted a direct structural determination of the concentration of active compared to inactive dopants, which were expected to differ by their coordination of four in contrast to three. However, the large experimental uncertainties and side effects such as dopant clustering or bonding to hydrogen[58–61] made these results difficult to interpret and lead to an overestimation of the doping efficiency. Therefore, Street and co-workers proposed to determine the doping efficiency from the number of excess charge carriers introduced by electronically active dopants compared to the undoped case.[10,11,49,62,63] To this end, one has to determine not only the concentration of electrons or holes in shallow states but also the densities of dangling bonds in their respective charge state, which compensate excess carriers. Combining the data from subgap absorption and EPR measurements, a quantitative analysis of the doping efficiencies $\eta(P)$ and $\eta(B)$ in a-SiO_x:H can be carried out (see Ref. 11 for details). Assuming that all negative defects in n-type SiO_x arise from the autocompensation and correspond to one active, fourfold coordinated P_4^+ donor [Eq. (1)], the doping efficiency of phosphorus in silicon suboxide can be calculated as follows:

$$\eta(P) = \frac{N_{D,Abs(n)} + N_{S(n)}(g=2.0040) - N_{S(n)}(g=2.0050)}{[\mathrm{P}]} \approx \frac{N_{D,Abs(n)} - N_{D,EPR(n)}}{[\mathrm{P}]}. \quad (6)$$

Here, $N_{S(n)}(g=2.0040)$ and $N_{S(n)}(g=2.0050)$ are the spin densities of electrons in the conduction-band tail and of neutral dangling bonds, respectively, and [P] is the solid-phase concentration of phosphorus atoms as determined by ERD (cf. Fig. 8). Similar arguments apply for boron-doped SiO_x, where every positive defect is assumed to arise from an active fourfold coordinated B_4^- acceptor:

$$\eta(B) = \frac{N_{D,Abs(p)} + N_{S(p)}(g\approx 2.007) - N_{S(p)}(g=2.0050)}{[\mathrm{B}]} \approx \frac{N_{D,Abs(p)} - N_{D,EPR(p)}}{[\mathrm{B}]}. \quad (7)$$

In this case, $N_{S(p)}(g=2.007)$ is the spin density of holes in the valence-band tail and [B] is the solid-phase concentration of boron atoms (cf. Fig. 8). Of course, $N_{D,EPR}$ in Eqs. (6) and (7) represents the undeconvoluted paramagnetic defect density and is only an approximation for the neutral dangling bond density. However, the absorption defect density $N_{D,Abs}$ (representing charged defects) is roughly one order of magnitude larger than $N_{D,EPR}$ for $E_{04} < 2.3$ eV or [O] < 30 at. %, respectively (cf. Fig. 14). This implies that for the calculation of the doping efficiencies, $N_{D,EPR}$ is almost negligible for those samples, where doping is still possible. Thus, the decrease of the doping efficiency is mainly determined by the decrease of $N_{D,Abs}$. For samples above [O] = 30 at. %, when doping fails, $N_{D,Abs}$ and $N_{D,EPR}$ become comparable and both represent neutral dangling bond defects.

For both, n- and p-type material, the doping efficiencies shown in Fig. 18 are in the range of 1% for low E_{04}, in good agreement with values obtained in previous studies.[10,11,63] With increasing optical band-gap, $\eta(P)$ and $\eta(B)$ decrease continuously, until they vanish above $E_{04} \approx 2.5$ eV ([O] $\approx$ 30 at. % or $\langle r \rangle \approx 3$). Thus, we can conclude that the change of conductivity and defect densities of doped SiO_x can be explained as a failure of substitutional P and B doping for higher oxygen contents. An average fourfold coordination of the network seems to be crucial for an effective dopant activation, which is no longer fulfilled for $E_{04} > 2.5$ eV where $\langle r \rangle$ approaches a value of 3. The decrease of η as a function of [O] indeed follows the probability $p(\mathrm{Si\text{-}Si_4})$, predicted from the random bonding model,[64] that a Si atom or a substitutional dopant atom is surrounded by four Si neighbors. For phosphorus and boron this represents the probabil-

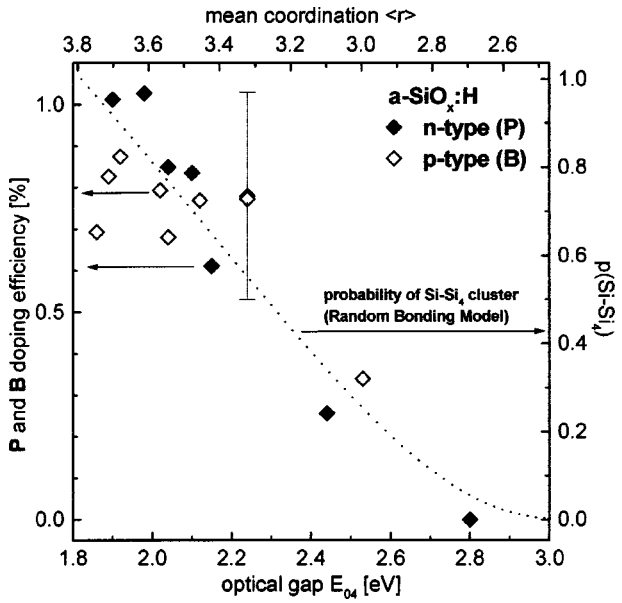

FIG. 18. Doping efficiency of phosphorus (1% PH_3, solid diamonds) and boron in a-SiO_x:H (2% B_2H_6, open diamonds) as a function of the optical band-gap E_{04} and average coordination $\langle r \rangle$. For comparison, the probability of Si—Si_4 clusters in a random network (dotted line) with increasing E_{04} is shown.

ity of finding a fourfold coordinated Si environment, which becomes more unlikely at higher oxygen contents (see Fig. 18).

An independent experimental indication that P can only be electrically active close to $\langle r \rangle = 4$ is the fact that in spin dependent photoconductivity (SDPC) measurements, the characteristic hyperfine lines of the neutral P_4^0 state could only be observed for small E_{04} and [O], respectively. Figure 19 displays SDPC spectra of n-type SiO_x for optical gaps up to 2.10 eV ([O]=12 at.%). The central resonance at $g \approx 2.004$ arising from conduction-band tail electrons is present in all of the spectra but only shown for the smallest E_{04}. The hyperfine-split lines due to neutral P_4^0 dopants[11,65] can also be seen with comparable intensity at 3210 and 3470 G and with a constant splitting of $\Delta H_{hf} \approx 260$ G in all of the spectra. For SiO_x samples with higher oxygen contents, the SDPC signal turned out to be too weak in order to measure reliable spectra. Figure 19 implies that although the oxygen content gradually increases and P_4 donors become more unlikely, the microscopic surrounding of the remaining active donors stays essentially unchanged, namely, Si-Si_4 clusters with $\langle r \rangle \approx 4$ (as shown schematically by the inset of Fig. 19).

Based on these results, it has to be asked whether the autocompensation model[10] is still a valid concept when a reduction of the mean coordination by alloying with increasing oxygen concentrations results in a decrease of the doping efficiency. Equations (1) and (2) propose an equilibrium between fourfold coordinated dopants D_4 compensated by an equal number of charged defects Si_3 on one side and threefold coordinated dopants D_3 together with fourfold coordinated Si_4 atoms ($[Si_4] \simeq$ const) on the other side. Applying the law of mass action yields, under the assumption of thermal equilibrium,

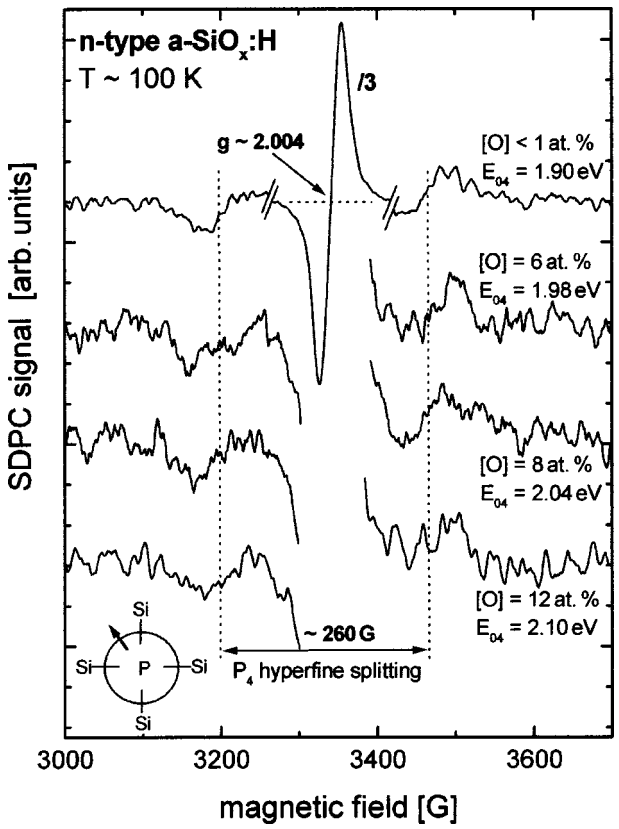

FIG. 19. Spin-dependent photocurrent spectra of phosphorus-doped a-SiO_x:H (1% PH_3) with $E_{04}=1.90$, 1.98, 2.04, and 2.10 eV. The central conduction-band tail resonance ($g \approx 2.004$) is plotted on a different intensity scale for one of the spectra. The positions of the hyperfine-split lines due to neutral P_4^+ dopants at roughly 3210 and 3470 G ($\Delta H_{hf} \approx 260$ G) are indicated by dotted straight lines.

$$\frac{[D_4]^2}{[D]} = \text{const} \tag{8}$$

with $[D_4]=[Si_3]$ and $[D_3] \simeq [D_{total}]=[D]$. For the doping efficiency η this leads to

$$\eta = \frac{[D_4]}{[D]} \simeq \frac{\text{const.}}{\sqrt{[D]}}. \tag{9}$$

Although Eqs. (1), (2), and (9) are able to explain most of the properties observed in doped samples, there are doubts about the general applicability of the autocompensation model, which have been summarized by Stutzmann *et al.*[11,63] First, the assumption of thermal equilibrium at the growing surface during deposition [Eqs. (1) and (2)] is incompatible with the growth process of an amorphous network. On the contrary, a rapid solidification of the material is required in order to prevent the atoms from attaining their minimum-energy configuration and crystallizing. As a consequence, some of the structural units found in amorphous silicon or germanium are in contradiction with the 8-N rule, even in Street's modified form. The most prominent examples are the neutral Si_3^0 or Ge_3^0 dangling bonds in undoped material. As a

matter of fact, amorphous silicon or germanium are not totally free of topological constraints. The overconstrainedness of the tetrahedral network leads to the formation of configurations which are forbidden in the picture of the autocompensation but might favor a substitutional incorporation of dopant atoms.

Second, it was observed that the doping efficiency shows a common unique square-root behavior [Eq. (9)] as a function of the gas-phase dopant concentration, whereas the situation is more complicated as a function of the solid-phase concentration.[11,63] For example, the doping efficiencies of As in *a*-Si:H and P in *a*-Ge:H do not show the expected decrease with the square root of the solid-phase dopant concentration, but remain rather constant. Note that Eq. (9) is written in terms of solid-phase concentration under the assumption of thermal equilibrium. In reality, however, gas-phase reactions and gas-surface interactions, such as the formation of plasma precursors and their following reaction with the growth surface, have a crucial influence on the doping efficiency in amorphous Si and Ge, thus violating the modified 8-*N* rule. Attempts have been made to include gas-phase species in the doping model of P-doped *a*-Si:H,[66] however, the model is too specialized to account for the doping process of all studied dopant-host systems. Thus, no general model for the dependence of the doping efficiency on gas- or solid-phase concentrations has been established so far and the understanding is restricted to the phenomenological explanations of the modified 8-*N* rule .

In the case of *a*-SiO_xH, the situation is further complicated by the presence of increasing amounts of oxygen atoms. There are two plausible explanations for the decrease of the *n*- and *p*-type doping efficiency with increasing [O] and decreasing mean coordination. The extent of the various contributions, however, is difficult to evaluate. On the one hand, the gradual reduction of topological constraints in the SiO_x matrix with decreasing $\langle r \rangle$ is likely to account for the decreasing fourfold coordinated active dopant incorporation. As mentioned above, the overconstrainedness of the network imposes certain constraints on possible configuration of the dopant atoms. Therefore, at $\langle r \rangle \approx 3$, dopant atoms will no longer be forced into fourfold bonding configurations, since only a few constraints are left in the matrix itself, which are unlikely to be sufficient to influence the incorporation of the respective dopant atom. In this picture, a successful doping process essentially depends on the existence of steric constraints, which are forbidden by the original 8-*N* rule.

On the other hand, the presence of oxygen and hydrogen and their possible bonding configurations have to be considered as well. Hydrogen-dopant passivation is a well-known phenomenon in crystalline semiconductors.[67] Furthermore, the strong electronegativity difference between oxygen and boron or phosphorus will lead to energetic positions of dopant-oxygen bonding and antibonding levels quite different from those of the corresponding silicon-dopant bonds. However, in *a*-Si:H and especially *a*-SiO_x:H neither signs of dopant-oxygen nor dopant-hydrogen bonding could be detected by IR spectroscopy for oxygen concentrations up to 20 at. %. Since the maximum hydrogen concentration is $\sim$20 at. % also for higher [O] (cf. Fig. 2), H passivation of phosphorus or boron is unlikely to play a major role even when the oxygen fraction rises because such complexes in crystalline silicon are not stable at the deposition and annealing temperatures employed in this study. Yet, dopant-oxygen binding might well contribute to an increasing dopant passivation and the decrease of η for $[O] > 20$ at. %.

Nevertheless, the steric constraints of the overcoordinated amorphous network are likely to have an influence on the efficiency of the doping process in tetrahedral amorphous materials. The presence of a significant amount of network constraints may help to understand why successful doping was so far observed only for the fourfold coordinated amorphous semiconductors *a*-Si:H, *a*-Ge:H, *a*-C:H, and their alloys, but fails upon alloying *a*-SiO_x:H with increasing amounts of oxygen.

VII. CONCLUSIONS

We have investigated the correlation between the structural and mechanical properties and the doping efficiency of hydrogenated amorphous silicon suboxides (*a*-SiO_x:H) as a function of the oxygen content (0–50 at. %) and optical band-gap ($E_{04} \approx 1.9$–2.8 eV). Alloying with increasing oxygen concentrations gives rise to a softening of the amorphous network by the two-valent O atoms and results in a linear decrease of the mean atomic coordination $\langle r \rangle$ from four (*a*-Si:H) to ≈ 2.7 for the highest oxygen concentrations studied (45 at. %). Thus, amorphous silicon suboxides undergo a structural change from an overconstrained amorphous semiconductor via a glassy semiconductor towards a semiconducting glass with increasing amounts of oxygen. However, $\langle r \rangle$ remains above the value for rigidity percolation known from network glasses.[3–5] Experimental results for the mechanical hardness of the material correlate well with this decrease of the average coordination.

Efficient phosphorus and boron doping in SiO_x seems to be related to the presence of local environments with fourfold coordination. For $[O] \leqslant 12$ at. %, active phosphorus dopants have similar wave functions and doping efficiencies around 1% as in *a*-Si:H. Also, large doping-induced densities of charged defects are found for low [O], as predicted by Street's modified 8-*N* rule.[10] Beyond $[O] = 20$ at. %, however, the dark conductivities, the absorption, and the EPR spectra exhibit increasingly intrinsic behavior: The concentration of charged dangling bonds decreases in favor of neutral Si_3^0 and the doping efficiency tends towards zero. For average coordination of three or less ($[O] \gtrsim 30$ at. %, $E_{04} \gtrsim 2.5$ eV), doping fails and all samples—doped and undoped—have intrinsic character. The phenomenological explanation provided by the autocompensation model[10] is unlikely to account for the details of the doping process in amorphous semiconductors. Inconsistencies are well known, such as the existence of topological constraints in the amorphous network or the fact that rather the gas-phase than the solid-phase dopant concentration determines the behavior of the doping efficiency.[11] In the case of *a*-SiO_x:H, where the tetrahedral coordination is successively reduced and the doping efficiencies of P and B decrease with rising [O], steric

constraints in local environments with $\langle r \rangle \approx 4$, though violating the modified 8-N rule, seem to be favorable for efficient substitutional doping. The reduced number of network constraints in silicon suboxides with increasing oxygen concentration might also explain the finding that doping in amorphous semiconductors has so far only been observed in overconstrained tetrahedral materials (a-Si:H, a-Ge:H, a-C:H, and their alloys).

ACKNOWLEDGMENTS

This work was supported by the Deutsche Forschungsgemeinschaft (DFG Project Stu. 139/6-3).

*Electronic address: janotta@wsi.tum.de; FAX: +49 89 289 12737.

[1] N.F. Mott, Adv. Phys. **16**, 49 (1967).
[2] N.F. Mott, Philos. Mag. **19**, 835 (1969).
[3] J.C. Phillips, Phys. Rev. Lett. **42**, 1151 (1979).
[4] J.C. Phillips, J. Non-Cryst. Solids **34**, 153 (1979).
[5] J.C. Phillips, J. Non-Cryst. Solids **43**, 37 (1981).
[6] D.K. Biegelsen, Sol. Cells **2**, 421 (1980).
[7] R.C. Chittick, J.H. Alexander, and H.F. Sterling, J. Electrochem. Soc. **116**, 77 (1969).
[8] W.E. Spear and P.G. LeComber, Solid State Commun. **17**, 1193 (1975).
[9] W.E. Spear, Adv. Phys. **26**, 811 (1977).
[10] R.A. Street, Phys. Rev. Lett. **49**, 1187 (1982).
[11] M. Stutzmann, D.K. Biegelsen, and R.A. Street, Phys. Rev. B **35**, 5666 (1987).
[12] J. Robertson, Phys. Rev. B **28**, 4647 (1983); **28**, 4658 (1983); **28**, 4666 (1983).
[13] B. von Roedern, L. Ley, M. Cardona, and F.W. Smith, Philos. Mag. B **40**, 433 (1979).
[14] W.B. Jackson, S.-J. Oh, C.C. Tsai, and J.W. Allen, in *Optical Effects in Amorphous Semiconductors*, edited by P. C. Taylor and S. G. Bishop, AIP Conf. Proc. No. 120 (AIP, New York, 1984), p. 341.
[15] A. Hadjadj, P. Roca i Cabarrocas, and B. Equer, Philos. Mag. B **80**, 1317 (2000).
[16] Z.E. Smith and S. Wagner, in *Amorphous Silicon and Related Materials*, edited by H. Fritzsche (World Scientific, Singapore, 1988), p. 409.
[17] K. Winer, Phys. Rev. Lett. **63**, 1487 (1989)
[18] K. Winer, Phys. Rev. B **41**, 12 150 (1990).
[19] M.J. Powell and S.C. Deane, Phys. Rev. B **48**, 10 815 (1993).
[20] M. Stutzmann, in *Handbook on Semiconductors*, edited by T. S. Moss and S. Mahajan (Elsevier Science B. V., Amsterdam, 1994), Vol. 3, p. 657.
[21] A. Bergmaier, G. Dollinger, and C.M. Frey, Nucl. Instrum. Methods Phys. Res. B **99**, 488 (1995).
[22] W.B. Jackson, N.M. Amer, A.C. Boccara, and D. Fournier, Appl. Opt. **20**, 1333 (1981).
[23] W.C. Oliver, G.M. Pharr, J. Mater. Res. **7**, 1564 (1992).
[24] P. Boolchand and M.F. Thorpe, Phys. Rev. B **50**, 10 366 (1994).
[25] J. Wells, W.J. Bresser, P. Boolchand, and J. Lucas, J. Non-Cryst. Solids **195**, 170 (1996).
[26] G.H. Döhler, R. Dandoloff, and H. Bilz, J. Non-Cryst. Solids **42**, 87 (1980).
[27] M.F. Thorpe, J. Non-Cryst. Solids **57**, 355 (1983).
[28] M.F. Thorpe and M.V. Chubynsky, in *Properties and Applications of Amorphous Materials*, Vol. 9, NATO *Science Series* II, edited by M. F. Thorpe and L. Tichý (Kluwer Academic, Dordrecht, 2001), p. 61.
[29] P. Boolchand, M. Zhang, and B. Goodman, Phys. Rev. B **53**, 11 488 (1996).
[30] J.C. Angus and F. Jansen, J. Vac. Sci. Technol. A **6**, 1778 (1988).
[31] R.L. Mozzi and B.F. Warren, J. Appl. Crystallogr. **2**, 164 (1959).
[32] R. Janssen, *Strukturelle und elektronische Eigenschaften amorpher Silizium-Suboxide*, Selected Topics of Semiconductors Physics and Technology, Vol. 31, edited by G. Abstreiter, M. C. Amann, M. Stutzmann, and P. Vogl (Walther Schottky Institute, Munich, 2000).
[33] A. Kelly and N. H. McMillan, in *Strong Solids* (Oxford University Press, Oxford, 1986).
[34] X. Jiang, B. Goranchev, K. Schmidt, P. Grünberg, and K. Reichelt, J. Appl. Phys. **67**, 6772 (1990).
[35] X. Jiang, K. Reichelt, and B. Stritzker, J. Appl. Phys. **66**, 5805 (1989).
[36] T. A. Hayes and M. E. Kassner, in *Properties of Amorphous Silicon and its Alloys*, edited by T. Searle, Emis Datareviews Series No. 19 (Inspec The Institution of Electrical Engineers, London, 1998), p. 363.
[37] M.S. Brandt, A. Asano, and M. Stutzmann, in *Amorphous Silicon Technology*, edited by E.A. Schiff, M.J. Thompson, A. Madan, K. Tanaka, and P.G. LeComber, Mater. Res. Soc. Symp. Proc. No. 297 (Materials Research Society, Pittsburgh, 1993), p. 201.
[38] W.Y. Ching, Phys. Rev. B **26**, 6633 (1982).
[39] R. Carius, R. Fischer, and E. Holzenkämpfer, J. Phys. C **4**, 1025 (1981).
[40] H.R. Philipp, J. Phys. Chem. Solids **32**, 1935 (1971).
[41] H.R. Philipp, J. Non-Cryst. Solids **8-10**, 627 (1972).
[42] E. Holzenkämpfer, F.-W. Richter, J. Stuke, and U. Voget-Grote, J. Non-Cryst. Solids **32**, 327 (1979).
[43] R. Carius, R. Fischer, E. Holzenkämpfer, and J. Stuke, J. Appl. Phys. **52**, 4241 (1981).
[44] M. Zacharias, H. Freistedt, F. Stolze, T.P. Drüsedau, M. Rosenbauer, and M. Stutzmann, J. Non-Cryst. Solids **164-166**, 1089 (1993).
[45] M. Stutzmann and C.E. Nebel, in *Encyclopedia of Applied Physics*, edited by G. L. Trigg (VCH Publishers, New York, 1997), Vol. 18, p. 151.
[46] H. Dersch, J. Stuke, and J. Beichler, Phys. Status Solidi B **105**, 265 (1981).
[47] H. Dersch, J. Stuke, and J. Beichler, Phys. Status Solidi B **107**, 307 (1981).
[48] S. Hasegawa, T. Kasajima, and T. Shimizu, Philos. Mag. B **43**, 149 (1981).
[49] R.A. Street, D.K. Biegelsen, and J.C. Knights, Phys. Rev. B **24**, 969 (1981).
[50] J.C. Knights, D.K. Biegelsen, and I. Solomon, Solid State Commun. **22**, 133 (1977).
[51] A. Friedrich and D. Kaplan, J. Electron. Mater. **8**, 79 (1979).
[52] H. Dersch and L. Schweitzer, Philos. Mag. B **50**, 397 (1984).

[53] J.C. Knights, T.M. Hayes, and J.C. Mikkelsen, Jr., Phys. Rev. Lett. **39**, 712 (1977).
[54] J.A. Reimer and T.M. Duncan, Phys. Rev. B **27**, 4895 (1983).
[55] S.G. Greenbaum, W.E. Carlos, and P.C. Taylor, Solid State Commun. **43**, 663 (1982).
[56] S.G. Greenbaum, W.E. Carlos, and P.C. Taylor, J. Appl. Phys. **56**, 1874 (1984).
[57] S. Hayashi, K. Hayamizu, S. Yamasaki, A. Matsuda, and K. Tanaka, Phys. Rev. B **38**, 31 (1988).
[58] J.B. Boyce and S.E. Ready, Phys. Rev. B **38**, 11 008 (1988).
[59] J.I. Pankove, D.E. Carlson, J.E. Berkeyheiser, and R.O. Wance, Phys. Rev. Lett. **51**, 2224 (1983).
[60] N.M. Johnson, R.D. Burnham, R.A. Street, and R.L. Thornton, Phys. Rev. B **33**, 1102 (1986).
[61] N.M. Johnson, C. Herring, and D.J. Chadi, Phys. Rev. Lett. **56**, 769 (1986).
[62] W.B. Jackson and N.M. Amer, Phys. Rev. B **25**, 5559 (1982).
[63] M. Stutzmann, Philos. Mag. B **53**, L15 (1986).
[64] K. Hübner, Phys. Status Solidi A **61**, 665 (1980).
[65] M. Stutzmann and R.A. Street, Phys. Rev. Lett. **54**, 1836 (1985).
[66] F.J. Kampas and P.E. Vanier, Phys. Rev. B **31**, 3654 (1985).
[67] S.J. Pearton, J.W. Corbett, and T.S. Shi, Appl. Phys. A: Solids Surf. **43**, 153 (1987).